Control and Modeling of the Dielectrophoretic Assembly of On-Chip Nanoparticle Wires

Ketan H. Bhatt and Orlin D. Velev*

Department of Chemical Engineering, North Carolina State University, Raleigh, North Carolina 27695-7905

Received June 5, 2003. In Final Form: September 24, 2003

Ⓦ This paper contains enhanced objects available on the Internet at http://pubs.acs.org/journals/langd5.

Suspensions of metallic nanoparticles in water were assembled via the action of an alternating electric field (dielectrophoresis) into wires of micrometer thickness. Two modes of microwire assembly, one through the bulk of the suspension and one as half-cylinders on the glass surface between the electrodes, were identified. The operating conditions responsible for the two assembly modes were recognized. The control of the process parameters allows making, for example, straight single connectors or massively parallel arrays of microwires on the surface of the chip, which can be extracted in dry form. The microwire assembly process was modeled using finite element electrostatic calculations. The direction of growth can be guided by introducing conductive islands or particles in the suspension. The experiments, supported by electrostatic calculations, show that the wires grow in the direction of highest field intensity, "automatically" making electrical connections to the objects between the electrodes. The results point the way to controlled dielectrophoretic assembly of nanoparticles into on-chip electrical connectors, switches, and networks.

I. Introduction

The assembly of colloidal particles into functional structures is an exciting area of research for potential nanotechnology applications. Traditional areas of colloid assembly deal with the crystallization of microparticles into colloidal crystals, which can be conducive, for example, to the fabrication of photonic materials.[1−4] More recently, the assembly of particles of nanometer size has attracted significant interest for applications such as sensors[5−7] and nanocoatings.[8,9] Not all assembly processes, however, offer the combination of speed, simplicity, low cost, and precision that would be desired for technologically feasible applications.

One tool for rapid assembly of micro- and nanoparticles is dielectrophoresis (DEP), the particle mobility and interactions imparted by an alternating electric field.[10−12] The use of external fields offers a combination of speed, easy control, and precision, which may not be readily available through the inherent particle−particle colloidal interactions. Electric fields have been used in the assembly of complex particles,[13,14] colloidal crystals,[15−23] biosensors,[5,6] and linear particle aggregates.[24−27] The use of alternating (ac) fields in dielectrophoresis, in particular, allows avoiding electroosmotic and electrolysis effects, which significantly limit the precision and usability of the direct current (dc) fields.

One process of specific interest to applications in electrical circuits and sensors, that we reported previously,[27] is the assembly of metallic nanoparticles into long wires of micrometer thickness. The metal particles of diameter 10−20 nm are assembled in millimeter to centimeter sized gaps between two planar electrodes on a surface. The long, porous fibrillar assemblies grow when the nanoparticles are attracted and aggregated by the DEP force at the end of the microwires. The microwires formed have good ohmic conductance for both ac and dc currents. They can form rudimentary self-repairing "wet" circuits and hold promise for applications in sensors, bioelectronic circuits, or other devices where electrical connectors are assembled *in situ* inside a liquid instead of being made by microfabrication.[27] A similar process has been recently used by others to assemble gold nanoparticles between nanometer spaced electrodes using

* To whom correspondence should be addressed. E-mail: odvelev@unity.ncsu.edu. Fax: 919-515-3465.

(1) Joannopoulos, J. D. *Nature* **2001**, *414*, 257.
(2) Braun, P. V.; Wiltzius, P. *Nature* **1999**, *402*, 603.
(3) Velev, O. D. In *Handbook of Surfaces and Interfaces of Materials*; Nalwa, H. S., Ed.; Academic Press: San Diego, CA, 2002.
(4) Velev, O. D.; Kaler, E. W. *Adv. Mater.* **2000**, *12*, 531.
(5) Velev, O. D.; Kaler, E. W. *Langmuir* **1999**, *25*, 3693.
(6) Park, S. J.; Taton, T. A.; Mirkin, C. A. *Science* **2002**, *295*, 1503.
(7) Moller, R.; Csaki, A.; Kohler, J. M.; Fritzsche, W. *Langmuir* **2001**, *17*, 5426.
(8) Norris, D. J.; Vlasov, Y. A. *Adv. Mater.* **2001**, *13*, 371.
(9) Lyon, L. A.; Musick, M. D.; Smith, P. C.; Reiss, B. D.; Pena, D. J.; Natan, M. J. *Sens. Actuator, B* **1999**, *54*, 118.
(10) Jones, T. B. *Electromechanics of particles*; Cambridge University Press: Cambridge, 1995.
(11) Pohl, H. A. *Dielectrophoresis*; Cambridge University Press: Cambridge, 1978.
(12) Pethig, R.; Huang, Y.; Wang, X. B.; Burt, J. P. H. *J. Phys. D: Appl. Phys.* **1992**, *24*, 881.
(13) Fuhr, G.; Müller, T.; Schnelle, T.; Hagedorn, R.; Voigt, A.; Fiedler, S. *Naturwissenschaften* **1994**, *81*, 528.
(14) Sides, P. J. *Langmuir* **2001**, *17*, 5791.
(15) Trau, M.; Saville, D. A.; Aksay, I. A. *Science* **1996**, *272*, 706.
(16) Giersig, M.; Mulvaney, P. *Langmuir* **1993**, *9*, 3408.
(17) Solomentsev, Y.; Bohmer, M.; Anderson, J. L. *Langmuir* **1997**, *13*, 6058.
(18) Gong, T.; Marr, D. W. M. *Langmuir* **2001**, *17*, 2301.
(19) Holgado, M.; Garcia-Santamaria, F.; Blanco, A.; Ibisate, M.; Cintas, A.; Miguez, H.; Serna, C. J.; Molpeceres, C.; Requena, J.; Mifsud, A.; Meseguer, F.; Lopez, C. *Langmuir* **1999**, *15*, 4701.
(20) Lumsdon, S. O.; Kaler, E. W.; Williams, J. P.; Velev, O. D. *Appl. Phys. Lett.* **2003**, *82*, 949.
(21) Gu, Z. Z.; Hayami, S.; Kubo, S.; Meng, Q. B.; Einaga, Y.; Tryk, D. A.; Fujishima, A.; Sato, O. *J. Am. Chem. Soc.* **2001**, *123*, 175.
(22) Hayward, R. C.; Saville, D. A.; Aksay, I. A. *Nature* **2000**, *404*, 56.
(23) Rogach, A. L.; Kotov, N. A.; Koktysh, D. S.; Ostrander, J. W.; Rogoisha, G. A. *Chem. Mater.* **2000**, *12*, 2721.
(24) Bezryadin, A.; Dekker, C.; Schmid, G. *Appl. Phys. Lett.* **1997**, *71*, 1273.
(25) Amlani, I.; Rawlett, A. M.; Nagahara, L. A.; Tsui, R. K. *Appl. Phys. Lett.* **2002**, *80*, 2761.
(26) Khondaker, S. I.; Yao, Z. *Appl. Phys. Lett.* **2002**, *81*, 4613.
(27) Hermanson, K. D.; Lumsdon, S. O.; Williams, J. P.; Kaler, E. W.; Velev, O. D. *Science* **2001**, *294*, 1082.

10.1021/la0349976 CCC: $27.50
Published on Web 11/05/2003

ac fields and then creating a small electrode gap by breaking the wire with dc currents.[26]

The magnitude of the dielectrophoretic force, F_{DEP}, which attracts the particles toward the tip of the growing wires is proportional to the gradient of the electric field intensity squared and is given by[10,11]

$$F_{DEP} = 2\pi\epsilon_1 \, \mathrm{Re}|K(\omega)|R^3\nabla(E^2)$$

where R is the radius of the particle, ϵ_1 is the dielectric permittivity of the medium, E is the electric field intensity, and K is the Clausius−Mossoti factor—the effective polarizability of the particle in media. The direction of the force is determined by the sign of the real part of K. For metallic nanoparticles in aqueous suspensions $\mathrm{Re}|K(\omega)| \approx 1$. This leads to positive dielectrophoresis, in which the gold nanoparticles are attracted toward the areas of high field intensity usually situated on the electrodes. Microwires begin assembling at the electrode surface due to the collective aggregation of the nanoparticles and continue to grow until they bridge the gap between the electrodes, resulting in a short circuit.

The use of such microwires in nanotechnology applications requires detailed understanding of the factors involved, and control over the assembly process, which have not been available to date. In this paper we describe the effect of different operating parameters on the assembly of nanoparticle wires and report methods to control the dielectrophoretic assembly process. We present iterative 2D electrostatic models for the microwire growth. The microwire structures and the growth direction predicted by these models are compared to what we observe experimentally. On that basis we propose methods to engineer specific microwire structures.

II. Materials and Methods

Substrate Fabrication. Glass microscope slides (Fisher Scientific, PA) were cleaned by immersing in Nochromix (Fisher Scientific, PA) solution overnight, and then they were washed thoroughly with deionized water from a Millipore RiOs system and dried in an oven at 60 °C. The dried slides were covered with Teflon Thread seal tapes (Fisher Scientific, PA) in areas where no electrodes were desired. The tapes act as masks when metal vapor deposition is carried out. A 10 nm layer of chromium was deposited on the glass first, to provide better gold adhesion to the substrate. A 100 nm gold layer was then deposited on top of the thin chromium layer. The distance between the two planar electrodes formed by this procedure can be controlled by varying the width of the masking tape. The gap for different electrodes was varied from 4 to 8 mm. For certain experiments, conductive islands were created in the gap between the gold electrodes by depositing spots of silver paint for electron microscopy (SPI Supplies, PA). The diameter of these conductive islands was varied from 1 to 3 mm.

Gold Nanoparticle Suspensions. Gold nanoparticle suspensions were prepared by the method of Slot and Geuze.[28] Auric acid (10 mL, 1 wt % in an 800 mL solution) was reduced with sodium citrate (40 mL, 1 wt % in a 200 mL solution) in the presence of tannic acid (100 μL, 0.1 wt %). Auric and tannic acids were purchased from Sigma Aldrich, MO. Sodium citrate was purchased from Fisher Scientific, PA. All chemicals were used as obtained. This process yields suspensions of 12−15 nm gold particles.

The concentration of gold nanoparticles as synthesized, $\approx 10^{12}$ particles/mL, was not sufficient for the microwire assembly experiments. The nanoparticle suspension was further concentrated by centrifuging at 1500g through Millipore BioMax filters (Fisher Scientific, PA). Before collecting the nanoparticles from the membrane, they were washed with distilled water to remove any remaining salts left from the reduction process. This process concentrated the suspension ≈100-fold to a nanoparticle concentration of $\sim 10^{14}$ mL^{-1}. Depending upon experimental conditions, the suspension was used as is or after further dilution. The gold nanoparticle concentration in the suspensions was determined by measuring the absorbance peaks at 520−525 nm with a JASCO V-550 spectrophotometer (JASCO Corporation, Japan). The absorbance peak for suspensions with gold concentration 10^{12} mL^{-1} (as synthesized by the Slot and Gueze method without further concentration) was around 1.1.

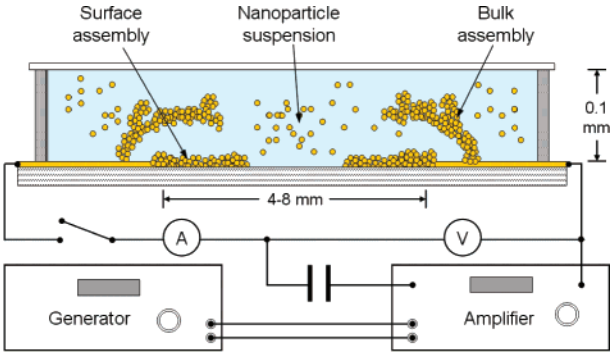

Figure 1. Outline of the experimental setup and schematics of the two different modes of microwire growth—bulk microwire assembly and surface microwire assembly. The chamber and the nanoparticle sizes are not to scale.

Experimental Setup. The nanoparticle suspension above the electrodes was contained in a 0.1 mm thick and 9 mm in diameter chamber created on the microscope slides by using SecureSeal imaging spacers (Grace Bio-Labs, OR). For some experiments the spacers were cut into stripes and the area of the chamber was kept at about 25−50 mm^2. Three to eight microliters of a concentrated gold nanoparticle suspension was loaded in the chamber, and it was sealed with a microscope glass cover slip.

The glass slide with the electrodes was then connected to the electrical circuit outlined in the bottom part of Figure 1. A FG-7002C Sweep/Function generator (EZ Digital Co., Ltd., Korea) was used as a source of square waves in the frequency range 100−3000 Hz. A RG-91 ramp generator/amplifier (Burleigh, NY) amplified the generated signal to the desired working voltage, 40−150 V. A 1 μF capacitor was included in the circuit to filter any direct current component of the signal. Digital multimeters connected in the circuit read the voltage applied and the current through the colloidal suspension. A master switch allowed starting and stopping the process whenever needed. The assembly process was continuously observed using an EMZ series zoom stereomicroscope (0.7−4.5× zoom, MEIJI Techno America, CA) and was recorded on a Toshiba PDR-M81 digital camera (Toshiba America, CA).

Electrostatics Calculations. To model the growth of microwires, we performed calculations of the electric field intensity. TRICOMP—a 2D electrostatics software package based on the finite element method—is freely available from Field Precision (Field Precision, NM; www.fieldp.com). The software includes a mesh generator MESH, an electrostatic calculator EStat, and an interactive results display module VEStat. In electrostatic calculations using the finite element method, the solution space is divided into a number of small elements. It is assumed that the properties within the element remain constant; hence, there are no elements shared between different objects or across boundary lines. Our calculations were performed on a mesh of variable isosceles triangles.

As the electric field has discontinuities at the surface of different dielectrics (which is the case of our problem, where water, glass, and gold electrodes have different dielectric constants), field calculations are carried out using the Poisson equation for the electric potential for each element

$$\nabla^2\phi = -\frac{\rho}{\epsilon_0}$$

where ϕ is the potential, ρ is the charge density (C/m^3), and ϵ_0 is the permittivity of free space (8.854×10^{-12} C^2/(J m)). The division of the solution space into small elements with constant

(28) Slot, J. W.; Geuze, H. J. *Eur. J. Cell Biol.* **1985**, *38*, 87.

properties allows linearizing the Poisson equation. The potential in any element is calculated by weighing out the potentials of its neighbors. The weighing factors are dependent upon the material properties (dielectric constants, conductivity) of the elements. The potential distribution for the solution space is obtained by iterative calculations. The field intensities are then calculated from the potential distribution. More details about the TRICOMP software and the finite element method are given in ref 29.

For all electrostatic calculations, detailed specifications of the electrode geometry and the surrounding regions (nanoparticle suspension, glass slide, cover slip) were provided as regions in a 2D plane to MESH to generate a variable triangular mesh. The physical properties of the materials, viz. dielectric constants, conductivity, and potential values, were specified into EStat, and numerical calculations were performed on the basis of the mesh generated. The solution matrix generated by EStat was viewed with VEStat in the form of plots of equipotentials and electric field lines for the whole system and for each element.

III. Experimental Results

The suspended metal nanoparticles began to aggregate and to form microwires when alternating electric fields were applied to the electrodes (Figure 1). The microwires grew through the nanoparticle suspension, until they bridged the gap and short circuited the electrodes. The aggregation of the metal nanoparticles is irreversible due to the strong van der Waals forces between them, and the assembled structures remained stable even after the voltage was turned off. The microwires were 1−2 μm in diameter and grew at assembly speeds up to 50 μm/s when alternating fields of 50−200 Hz and 50−250 V were applied.

Modes of Microwire Growth. We identified and characterized two qualitatively different modes of microwire assembly. These two assembly modes are referred to hereafter as bulk microwire assembly and surface microwire assembly. In the bulk microwire assembly, wires grew through the bulk of the suspension, as described in the earlier report.[27] The second mode of microwire assembly, where the wires grew directly on the glass surface, has not been previously reported. The nanoparticles in these surface-supported wires aggregated in half-cylinders, compared to the cylindrical aggregation in the bulk. The two types of structures could be easily distinguished by high magnification optical microscopy, as the surface microwires were always in the focal plane at the plate surface, while parts of the bulk ones might be out of focus, and the surface of the plate was not seen concurrently. Experimental images of bulk and surface microwires are shown in Figure 2.

The first major challenge of this work was to understand and control the mode of growth. In many of the initial experiments, surface or bulk wires began assembling without a clearly distinguishable trigger, and sometimes both types grew simultaneously. If the wire assembly began as bulk, it continued in bulk mode until there was a short circuit in the chamber. If the wire assembly began on the surface, it usually continued on the surface for most of the distance; however, at small separations between the tips of the microwires growing from opposite electrodes, the assembly mode often switched from surface to bulk.

The parameters used to characterize the microwire growth in the two modes were the assembly speed and the surface density. The assembly speed was determined by following the growth process in real time with a microscope. The microscope eyepiece scale marks were aligned with the electrodes, and the microscope zoom was adjusted so that the scale length was equal to the electrode gap. The distances covered by microwires growing from the two electrodes were recorded. The data for microwire growth were plotted in coordinates of percentage electrode gap covered versus time. The assembly speed was then calculated from the slope of the data in the plots.

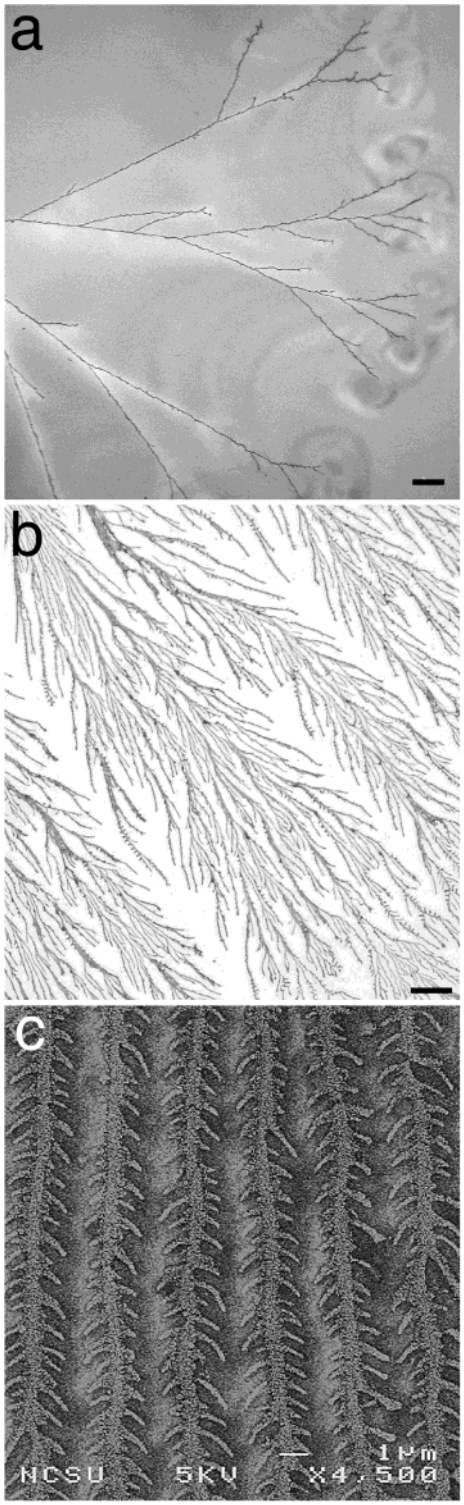

Figure 2. Typical experimental images of the two types of microwire structures obtained. (a) Bulk microwire growth. Note that some of the branches are not in the focal plane. (b) Surface microwires. (c) Scanning electron micrograph of the surface microwire structure. Scale bars: (a) 100 μm; (b) 20 μm.

Surface density is used as a qualitative parameter based on an estimate of the fraction of the total area covered by the microwires when viewed from the top after the

(29) Humphries, S. *Field Solutions on Computers*; CRC Press: Boca Raton, FL, 1998.

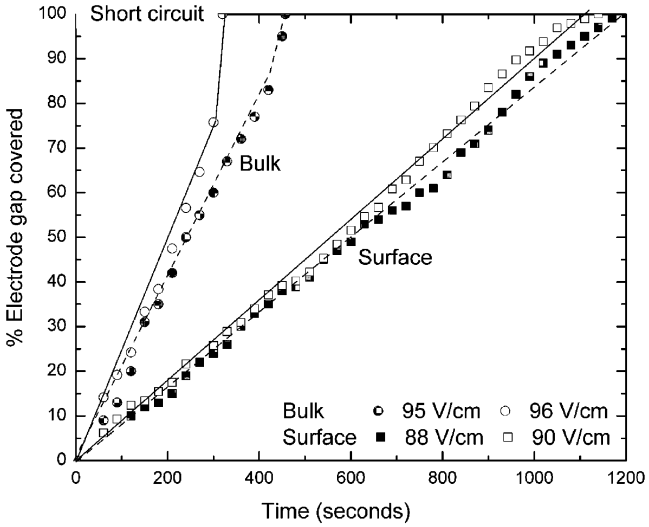

Figure 3. Speed of microwire assembly in bulk and surface modes plotted as percentage of electrode gap covered versus time. Two microwires were grown in each assembly mode to evaluate the reproducibility of the process. Lines are guides to the eye.

assembly process has been completed and the electrodes have short circuited. It effectively combines the degree of branching, the thickness, and the number of microwires formed into one parameter. Surface density will increase with an increase in any of the above individual parameters. The surface density of the bulk microwire structures was found to be always smaller than the one of the surface microwires (see Figure 2a and b).

Typical plots of the assembly process for bulk and surface microwire assembly are shown in Figure 3. The data are for four different experiments carried out on the same glass slide with a gap between the electrodes ≈5 mm. The concentration of gold nanoparticles was $\approx 2.23 \times 10^{13}$ mL^{-1}. The microwires grew through the bulk suspension when the initial voltages applied were 95 and 96 V/cm at a frequency of 1200 Hz. When the initial voltage was decreased to 90 and 88 V/cm, the microwires grew in the surface assembly mode. The data from Figure 3 also illustrate that the microwire assembly speed is well reproducible as long as the wires grow in the same mode, surface or bulk. The assembly speed for bulk microwires in this and other similar experiments was always higher than that for surface microwires (cf. the slope of the lines in Figure 3). The highest recorded assembly speeds of bulk microwires were 50 μm/s, and the highest speeds of surface microwire growth were 20 μm/s.

The most intriguing feature of the data displayed in Figure 3 is the linear relationship between the time elapsed and the gap covered. Thus, the microwire growth speed does not depend on the electric field intensity, which increases monotonically during the process as the distance between the tips of the wires from opposing electrodes decreases. This points out that the assembly process is controlled by a diffusion-limited or a diffusion-like process where the wire grows after enough nanoparticles are transported to its ends. The macroscopic structures obtained are similar to those observed for electric field induced diffusion-limited aggregation of microspheres.[30,31] The only evidence of a "reaction-controlled" regime is seen at low field intensities, where, as reported in our earlier paper, the microwire assembly starts abruptly only above a certain "threshold" intensity, where the field is strong enough to initiate aggregation.[27] In the cases studied here, the formation of microwires can be interpreted as collective aggregation of gold nanoparticles that have diffused to the areas of high electric field intensity (the electrodes and the tips of the growing microwires). As the mass transfer process is driven by the external ac field, any parameter that changes the forces acting on the particles will modulate the speed and specifics of the growth process. The effect of a number of such parameters, including frequency, electrolyte concentration, viscosity, and dielectric constant of the media, is presented in the next subsection.

The process is also influenced by the electrohydrodynamic fluid motion in the cell, which increases substantially at high field intensities. The observed transition of microwires from surface to bulk growth mode as the wires from the opposing electrodes approached each other was usually accompanied by intensive circulation of the fluid near the tips of the microwires, indicating substantial electrohydrodynamic flow. This surface to bulk mode transition could be prevented by decreasing the applied voltage (V) as the growing ends approach each other, which could be done by running the experiment at constant currents. This suppressed the electrohydrodynamic motion, and we obtained uniform surface wires in the electrode gap.

Effect of Operating Parameters on Assembly Speed of Microwires. The next experimental goal was to identify the parameters which affect the microwire assembly process and to characterize their effect on microwire growth. We also sought to identify conditions under which only bulk or surface microwires would grow. These data allowed us to achieve control of the microwire assembly process and to obtain microwire structures of a specific type.

The parameters which were recognized to control the growth of microwires were frequency, the concentration of electrolyte in the suspension, the viscosity and dielectric constant of the media, and the concentration of particles in the suspension. The effect of some of these parameters on the growth process is shown in Figure 4 by typical plots of microwire assembly evolution under different conditions. The experimental details and conclusions for all parameters studied are outlined below.

Effect of Electrolyte Concentration. A 0.1 mM NaCl solution was added to gold nanoparticle suspensions, and microwire formation was studied simultaneously for suspensions with and without added electrolyte (Figure 4a). To exactly duplicate the experimental conditions for the two systems being compared, we simultaneously loaded the two suspensions in two adjacent chambers on the same glass slide and thus followed parallel growth under identical conditions of an electric field of 80 V/cm at 1200 Hz applied across a ≈5 mm electrode gap. In both chambers the microwire formation began in the surface assembly mode and then transited to bulk as the wires approached each other. As demonstrated by Figure 4a, the addition of electrolyte increased the speed of growth for surface microwires. The assembly speed of the surface microwires decreases in the "depletion" region in Figure 4a because by this point of the process most of the particles in front of the growing wires have been depleted. The decreased concentration of gold nanoparticles in the suspension in front of the growing tips is easily observed optically, since the suspension color becomes less intense.

The increase of the speed of surface assembly in the presence of electrolyte correlates to the increase of the speed of bulk assembly with electrolyte reported earlier.[27]

(30) Wen, W.; Lu, K. *Phys. Rev. E* **1997**, *55*, R2100.
(31) Wen, W.; Zheng, D. W.; Tu, K. N. *Phys. Rev. E* **1998**, *58*, 7682.

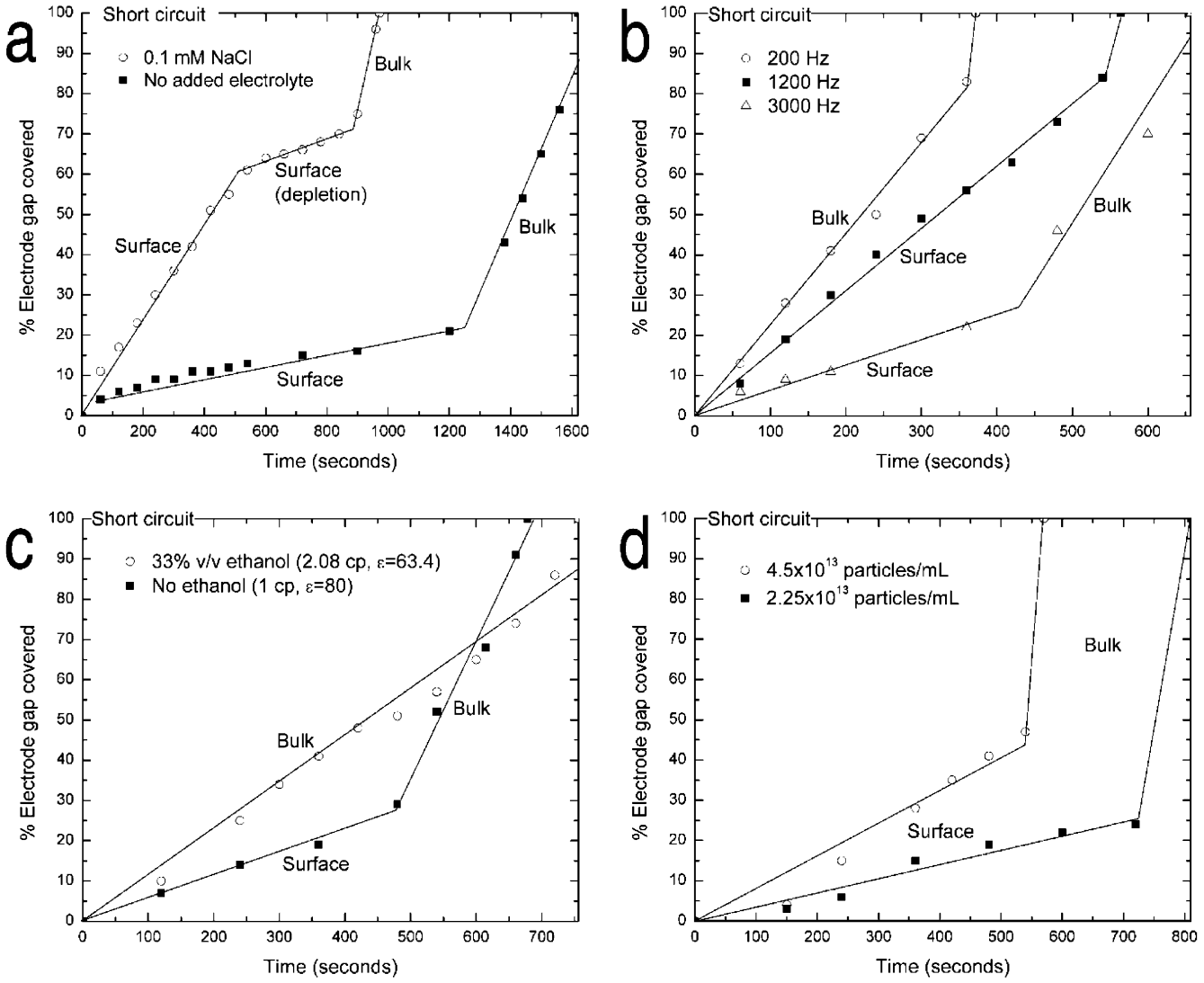

Figure 4. Effect of the operating parameters on the assembly speed of microwires: (a) electrolyte; (b) frequency; (c) viscosity and dielectric constant of the medium; (d) particle concentration. In all experiments the other parameters were kept constant. Note that in all plots the growth speed for bulk assembly is higher than that for surface assembly. Solid lines are guides to the eye.

The effect of electrolyte can be explained in terms of the suppression of the repulsive electrostatic interactions between the gold nanoparticles. The nanoparticles in our suspension are stabilized by the inherent negative surface changes only, as no surfactants or thiols were added. In the presence of electrolyte, the electrostatic repulsion between the gold nanoparticles is suppressed; however, the attractive van der Waals interactions remain the same. The aggregation of gold nanoparticles into microwires is thus facilitated and the assembly speed increases.

Effect of Frequency. Frequency was found out to be an important switch in controlling the mode of microwire growth. At frequencies close to 100 Hz, the microwires grew only in bulk assembly mode. At frequencies ≥ 1000 Hz, the wires grew predominantly in the surface assembly mode.

The data from experiments performed at three different frequencies while keeping all other parameters the same are plotted in Figure 4b. The field intensity was 110 V/cm, and the electrode gaps were approximately 5 mm. The microwire grew in the bulk assembly mode at 200 Hz. At 1200 and 3000 Hz, the wire growth started on the surface and transited to bulk as the two tips approached each other and the intensity increased. The assembly speed of the bulk microwires remained approximately constant at different frequencies. Frequency, however, had an effect on the assembly speed of the surface microwires, which decreased as frequency was increased.

We hypothesize that the decrease in the speed of growth with the increase in the frequency is related to the suppression of the displacement of the counterionic atmosphere around the particles and the resulting decrease of the dielectrophoretic force. The gold nanoparticles in the suspension are negatively charged and surrounded by counterions. This counterionic atmosphere is a source of additional dipolar polarization under the action of an electric field. When an external field is applied, the atmosphere moves in the direction opposite to the one of the charged particle, effectively resulting in the formation of a dipole. The reorientation of the dipoles to match the phase of the alternating electric field is limited by the relatively slow mobility of the counterions surrounding the particles. At higher frequencies the counterions cannot follow the rapidly oscillating field and the dipole polarization and interaction with the electric field decrease.[32] This is the likely reason for the decrease of the microwire growth

(32) Hunter, R. J. *Foundations of Colloid Science*, 2nd ed.; Oxford University Press: Oxford, 2001.

Table 1. Effect of Different Operating Parameters on the Assembly Speed and the Surface Density of Microwire Growth in Bulk and Surface Assembly Modes (↑ = Increases, ↓ = Decreases, − = No Change)

parameter	range	type	assembly speed	surface density
frequency ↑	100−3000 Hz	bulk	−	−
	1000−3000 Hz	surface	↓	↓
viscosity of media ↑	0.9−6.50 cP	bulk	very rapid formation of a single wire	
		surface	no surface growth seen at high viscosities	
dielectric constant of media ↑	60−80	bulk and surface	↑	−
particle concentration ↑	10^{13}−10^{15} mL^{-1}	bulk and surface	↑	−
electrolyte concentration ↑	0−0.1 mM	bulk and surface	↑	−

speed at higher frequencies. These data show that while the conductive metal cores of the gold nanoparticles are easily polarizable, the polarization of the counterionic atmosphere possibly also contributes to the dielectrophoretic attraction and microwire assembly. The counterionic polarization can also be suppressed by increasing the viscosity, as discussed below.

Effect of Media Viscosity and Dielectric Constant. The effect of the frequency on the microwire assembly shows the importance of the counterionic mobility as a source of field induced dipoles. The ionic mobility can also be suppressed by changing the viscosity, and thus, viscosity was expected to be a major controlling parameter for this process. It is difficult to distinguish the effect of the viscosity of the medium and the effect of the dielectric constant of the medium from each other. Addition of almost any liquid to the water-based suspension will decrease its dielectric constant. On the other hand, the viscosity may increase or decrease depending upon the properties of the liquid added. To characterize the effect of medium properties, we prepared samples containing 33% ethanol by volume and 50% glycerol by volume. The dielectric constants for both of these mixtures are the same and ≈63.4.[33] The ethanol based suspension has a viscosity of about 2.08 cP whereas the glycerol based suspension has a viscosity ≈6.5 cP.[33] The concentration of gold nanoparticles was kept constant in all suspensions.

Suspensions Containing Ethanol. The speed of growth in bulk assembly mode in ethanol−water suspensions was lower than that in normal aqueous suspensions (Figure 4c). This could be readily explained by the lower dielectrophoretic force at lower media permittivity (see the formula for F_{DEP}) and the higher viscosity of the medium.

Suspensions Containing Glycerol. This media has the same dielectric permittivity as ethanol, but three times higher viscosity. The more viscous media had a drastic effect on the microwire assembly, to the point where the mechanism of growth changed significantly. First, three to four times higher voltage was required for initiation of the microwire growth. Even at these higher fields, the microwires began to grow only after an initial induction period of about 1 min. However, once the process began, the wires grew with assembly speeds as high as 2 mm/s and short circuited in a matter of seconds. The formation of these wires was always in the bulk, and surface growth was never observed. The most intriguing and practically important characteristic of these glycerol-based microwires is that they are single, without branching, and very straight (more details are provided in section V below).

Our observations suggest that the mechanism of the assembly process for glycerol-based suspensions is different from that in aqueous suspensions. The higher viscosity of glycerol does not readily allow the nanoparticles to quickly diffuse and aggregate in the areas of high intensity. Instead, it appears that the nanoparticles slowly accumulate near the electrodes of the slide or near the periphery of the chamber (optically observed by intensification of the suspension color in these areas). The growth then proceeds at a high rate inside the highly concentrated nanoparticle phase (this could be seen as a transition to a "reaction-controlled" process, as the particles are preconcentrated at the electrodes and the mass transfer to the growing wire is very fast). The exact mechanism of this process will be a subject of our future investigations.

Table 2. "Switching Parameters" Identified that Allow Controlling the Mode of Microwire Assembly, Bulk or Surface

parameter	bulk	surface
frequency	100 Hz	1000 Hz
viscosity of media	1:1 glycerol−water (∼6.5 cP)	water-like (1 cP)
field strength	surface to bulk transition at increased field strengths	

Effect of Nanoparticle Concentration. The effect of gold particle concentration on the microwire assembly speed was straightforward. The assembly speed of the microwires directly increased with an increase of the concentration of gold nanoparticles in the suspension (Figure 4d). The same was true for the effect of field strength, which always increased the speed of microwire growth and was not investigated in detail here. A summary of the effect of the different parameters on the assembly speed and the surface density of microwire growth is presented in Table 1, and the key switching parameters between bulk and surface growth have been identified in Table 2.

IV. Modeling of the Microwire Growth Process by Electrostatics Calculations

The microwire assembly is driven by the electric field acting between the electrodes. Controlling of the process requires understanding of the role of this field in microwire formation, branching, assembly mode, and direction of growth. To achieve this, we performed two types of electrostatic calculations and modeling. In the first one, we focused on the local assembly process by calculating the field distribution at the growing tip of the microwire. These calculations provided information on the structure and branching of microwires and the mode of microwire assembly. To capture the effect of the chamber walls on the wire structure and growth mode, these calculations were performed in the vertical plane perpendicular to the chamber. Second, to predict the general direction of growth in the thin chamber, electrostatic calculations were performed in the horizontal plane of the chamber. These calculations were used to determine the direction of microwire growth on the basis of the electrode structure and in the presence of conductive elements in the gap. All calculations were performed on symmetrical systems with constant applied field.

Mechanism of Assembly. The schematics of the iterative algorithm used for modeling the dynamics of microwire growth in both bulk and surface assembly modes are shown in Figure 5. This algorithm is based on the fact that as the dielectrophoretic force pulls the gold nanoparticles along the direction of the electric field gradient,

(33) Madelung, O.; Wohlfarth, C. *Numerical Data and Functional Relationships in Science and Technology*; Landolt-Bornstein: Group IV; Springer-Verlag: New York, 1991.

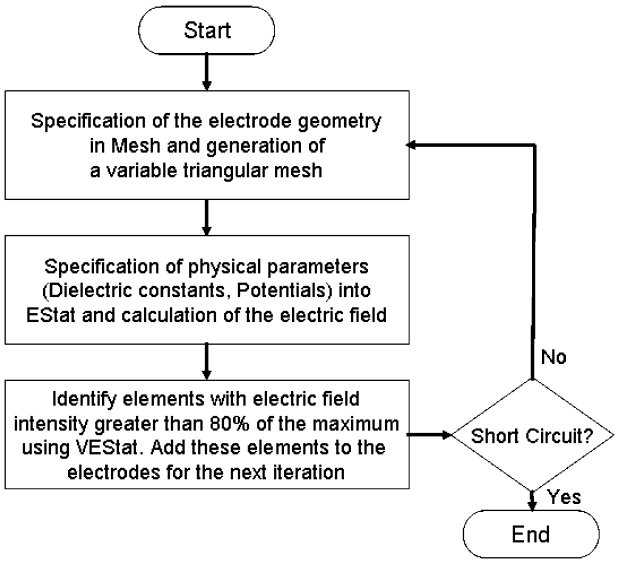

Figure 5. Algorithm for electrostatic simulation of the mechanism of microwire growth.

they will end up in the areas of highest electric field intensity. The growth will occur in these areas of high intensity. In general, this is the reason the particles accumulate at the tips of the microwires, where the field intensity is the highest.

We assumed that, at any stage of microwire growth, the nanoparticles will fill up the areas with highest field intensity. The initial electric potential solution was generated by EStat, and the field intensity inside each element of the triangular mesh was calculated by VEStat. At the next stage of the iterative procedure, all elements with field intensity empirically chosen to be higher than 80% of the maximum were identified (the change in the threshold intensity changes the scale, but not the pattern of growth). In the third step these elements were added to the microwires as newly assembled elements. At this step, we also filled up occasional empty mesh triangles between the new elements added and the metal structure to maintain a consistent microwire shape. The file with the coordinates of the new geometry of the system was then passed on to MESH to generate a variable triangular mesh, and then it was passed back to EStat to perform the next electrostatic calculation for the new geometry, and so on. The iterations were repeated until the wires short circuit.

The results of the iteration procedure were in remarkable agreement with the experimental data. The simulations demonstrate the formation of two opposing wires with multiple periodic large and small branches, which grow toward each other and short circuit at the end of the process. Snapshots of the electrode assembly at various intervals during modeling process for bulk (Figure 6a−g)

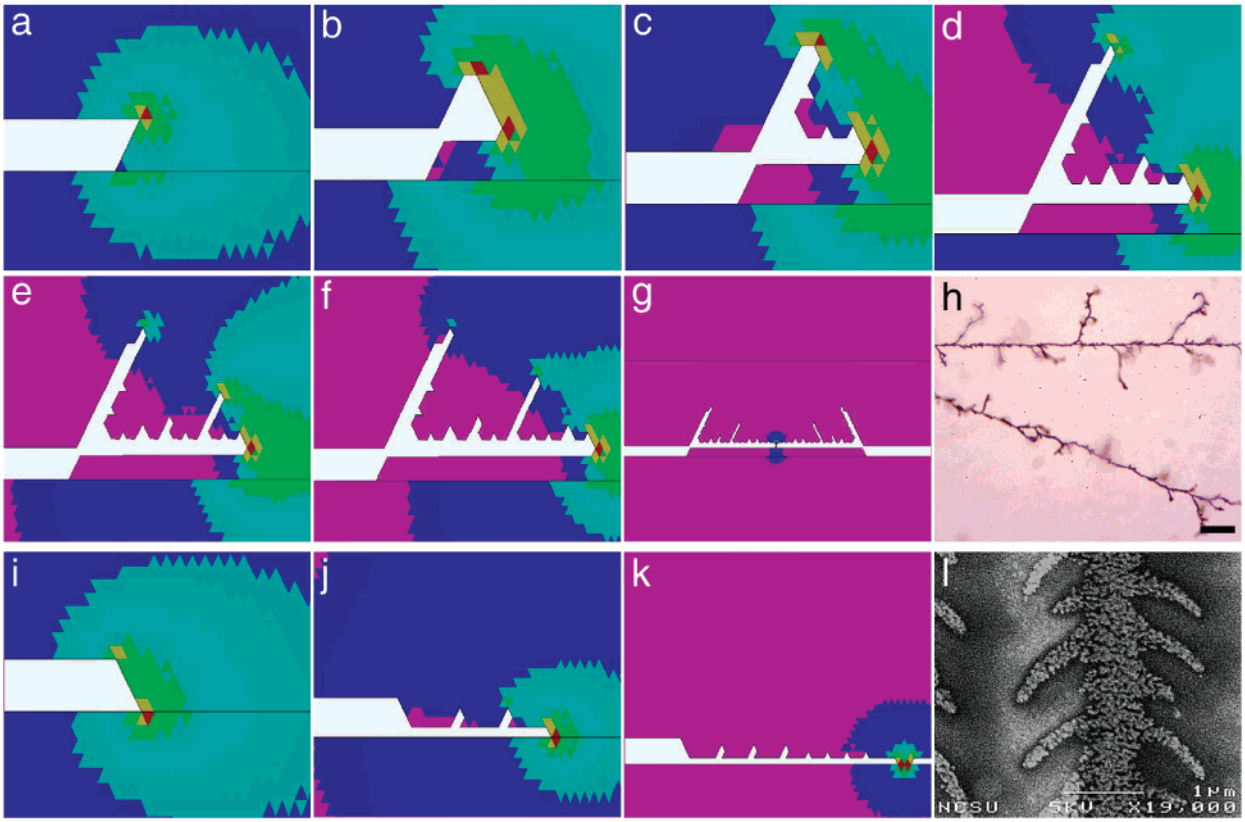

Figure 6. Snapshots of the results of the simulation process at various growth stages for both bulk and surface microwire assembly compared with actual experimental images. Bulk microwire assembly: (a) initial geometry; (b) branching of the wire; (c and d) propagation of branches; (e) the field intensity at the tip of the first branch drops below 80% of the maximum, leading to termination; (f) the first branch stops growing; (g) short circuit of the wires growing from opposing electrodes. Surface microwire assembly: (i) initial geometry; (j) the wire stays on the surface and does not form long branches; (k) wires are still on the surface even though nearing short circuit. The electrode and the microwires formed are shown in white, and the solid line next to the electrode delineates the suspension and the glass surface. Actual experimental images: (h) branching pattern for bulk microwires; (l) scanning electron micrograph of surface microwires. Compare parts g and h and k and l. Note that a slight change in the initial geometry (a and i) changes the assembly mode. Scale bar: 10 μm.

Ⓦ Movies of Ⓦ the bulk microwire simulation and Ⓦ the suface microwire simulation are available in AVI format.

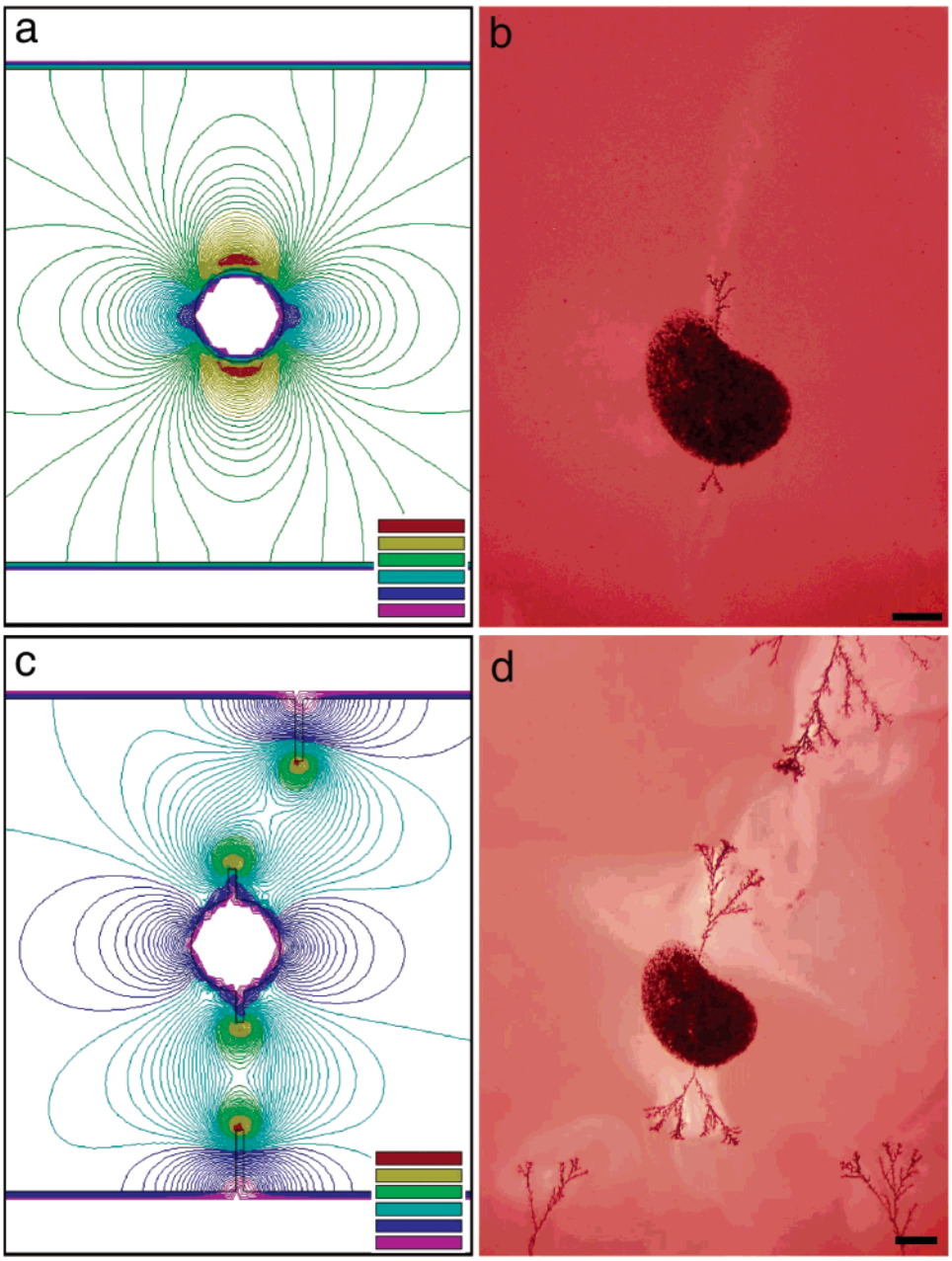

Figure 7. Electrostatic calculations around conductive objects compared with experimental images: (a) electric field intensity in the presence of a conductive island between planar electrodes; (b) actual experimental image proving that the wire growth starts at the island; (c) electrostatics calculations for wires growing from the island and from opposing electrodes, indicating that they will grow toward each other and short circuit; (d) experimental image depicting a situation similar to that in part c. Scale bars: 500 μm.

and surface (Figure 6i−k) microwire assembly are compared with actual experimental images in Figure 6.

To initiate the computational procedure for bulk microwire assembly, only a small slant away from the glass surface in the initial electrode geometry was required (Figure 6a). The electric field distribution at the end of the first iteration for bulk microwire assembly displayed in VEStat is shown in Figure 6a. The highest intensity of the electric field is near the edge of the electrode, as indicated by the bright red triangle element of the mesh used in the electrostatic calculations. The elements with electric field intensity equal to or greater than 80% of the maximum for this iteration are the red triangle and the two surrounding yellow triangles. These elements are added to the electrode geometry for the next iteration. The elements between the electrode and the red and yellow triangles are added as well to maintain the microwire structure. As the bulk wire grows, it widens and the electric field intensity distribution splits the wire into two different branches (Figure 6b and c). Branches continue to grow as long as the electric field intensity of the elements near the tips is high enough. Once the branches are left behind the growing wire and the field intensity on their tips decreases, they stop growing (Figure 6d−f). The pattern of branches for the simulated structure of bulk microwire indicates large branches with some smaller branches in between. The results of this simulation match very well the branching patterns observed experimentally in typical bulk microwires (Figure 6h).

To initiate the computational procedure for the surface microwires, the edge of the electrode was slanted toward the surface of the glass plate (Figure 6i). In this specific geometry the highest intensity element is located in the glass slide (red triangle in Figure 6i). This reflects the

physical law that the electric field intensity is higher in media with lower dielectric permittivity, which in this case is the glass slide (the dielectric permittivities of glass and water are 4.0 and 80, respectively). The local gradient of the field points toward the glass surface, and the particles will be accumulated there. The wire proceeds to propagate on the surface (Figure 6j and k). The branching structure observed in the scanning electron micrograph of the surface microwire at high magnification (Figure 6l) is similar to the one predicted by the modeling. Thus, simulations explain the periodic branching and the termination of growth once the branches are left behind the areas of high field intensity. More importantly, they prove that the mode of growth, bulk or surface, depends on minute differences in original conditions, which may be imperceptible in the actual experiment. This immediately explains why in the majority of experiments we observed random assembly of both types of wires, without a clear trigger for the formation of either type.

The switching parameters favoring the growth of microwires in the bulk or on the surface, which we identified, are likely to operate via more complex mechanisms, not taken into account here. For example, low frequency is likely to favor bulk growth by disruption of the surface growth by the electrohydrodynamic motion of the liquid in the vicinity of the glass wall. The existence of fluid movement near the electrode for DEP has been shown to displace particles away from the electrode at low frequencies.[34]

Predicting Microwire Growth around Conductive Objects. We have demonstrated in our earlier paper that microwires will "automatically" connect to any conductive objects present between the electrodes.[27] This is a potentially useful property of this process, as the microwires can be used as a tool to make *in situ* connections to objects in liquid-filled chambers and thus make electric circuits by field-driven assembly. To understand why the microwires grow toward these objects in the gap and how to direct the growth, we carried out simultaneous experiments and calculations of the electric field in the chamber.

In the experiments, conductive "islands" of silver paint were deposited on the glass slide between the electrodes. Microwires were then grown inside the chamber to investigate the effect of the islands on the wire formation and growth direction. In the supporting electrostatic calculations, the field intensity in the chamber with a conductive object in the middle was calculated. The results of electrostatic calculations compared with actual experimental images are shown in Figure 7.

The calculated intensity of the electric field is highest around the object. On the basis of the model for growth in the areas of highest intensity, this result suggests that the wire formation will start from the island. Such a theoretical prediction is somewhat counterintuitive, as it expects that the wires would begin assembling at the island that is not electrically connected, instead of at the electrodes where the field originates. However, it was directly confirmed by experiments such as the one shown in Figure 7b, where images of the initial stages of wire formation from a conductive island are captured. Thus, the DEP-based model of microwire assembly was proved and its predictive power was established. For example, when the microwires growing from the islands, and the ones from the electrodes, are displaced, the calculations show that they will grow toward each other and short circuit (Figure 7c). A similar situation is evident from the actual experimental image shown in Figure 7d. Thus, whenever there is a conducting object between the electrodes, the wires are very likely to spontaneously connect to it and include it in the circuit. This provides a useful tool for the *in situ* assembly of circuits, which is discussed in more detail in the following section.

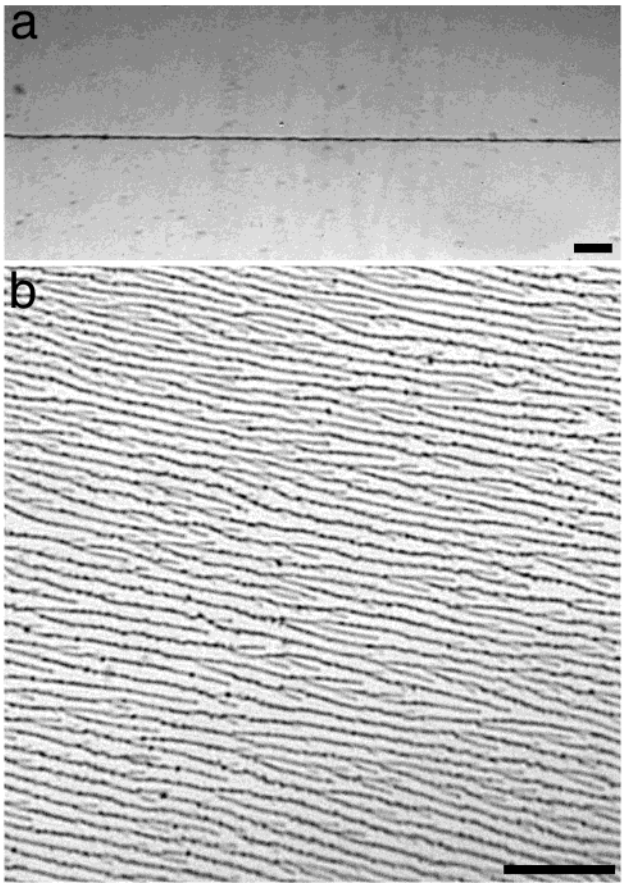

Figure 8. Controlled assembly of microwires with a specific morphology: (a) single unbranched microwire grown through the bulk nanoparticle suspension containing 50% glycerol by volume; (b) array of parallel wires assembled on the surface of a glass slide. Scale bars: 50 μm.

V. Engineered Microwire Assembly for Nanotechnology Applications

The assembly of electrically functional structures from suspensions of gold nanoparticles under the action of ac fields can be useful in various applications such as chemical sensors, "wet" electronic circuits, interfacing biological cells or tissues with electric systems, and so forth. The results of this work allowed us to take the first steps toward the control of the microwire growth process and the engineering of structures with specific functionality.

After understanding the effect of various parameters on microwire formation and with the help of electrostatic calculations, we were able to control the growth process to get desired microwires of specific structure. Figure 8a shows how a single, straight, and unbranched microwire could be grown through the bulk of the suspension. This wire was obtained at a frequency of 1000 Hz in suspensions containing 50% glycerol by volume. Alternatively, we can make the microwires on the surface assemble in the form of multiple parallel arrays. Figure 8b shows surface microwires grown parallel to each other. These wires were obtained at a frequency of 1200 Hz, an electrode gap of 5 mm, an area of the chamber $\approx$20 mm^2, and a 75 V/cm initial applied electric field, which was gradually decreased

(34) Ramos, A.; Morgan, H.; Green, N. G.; Castellanos, A. *J. Phys. D: Appl. Phys.* **1998**, *31*, 2338.

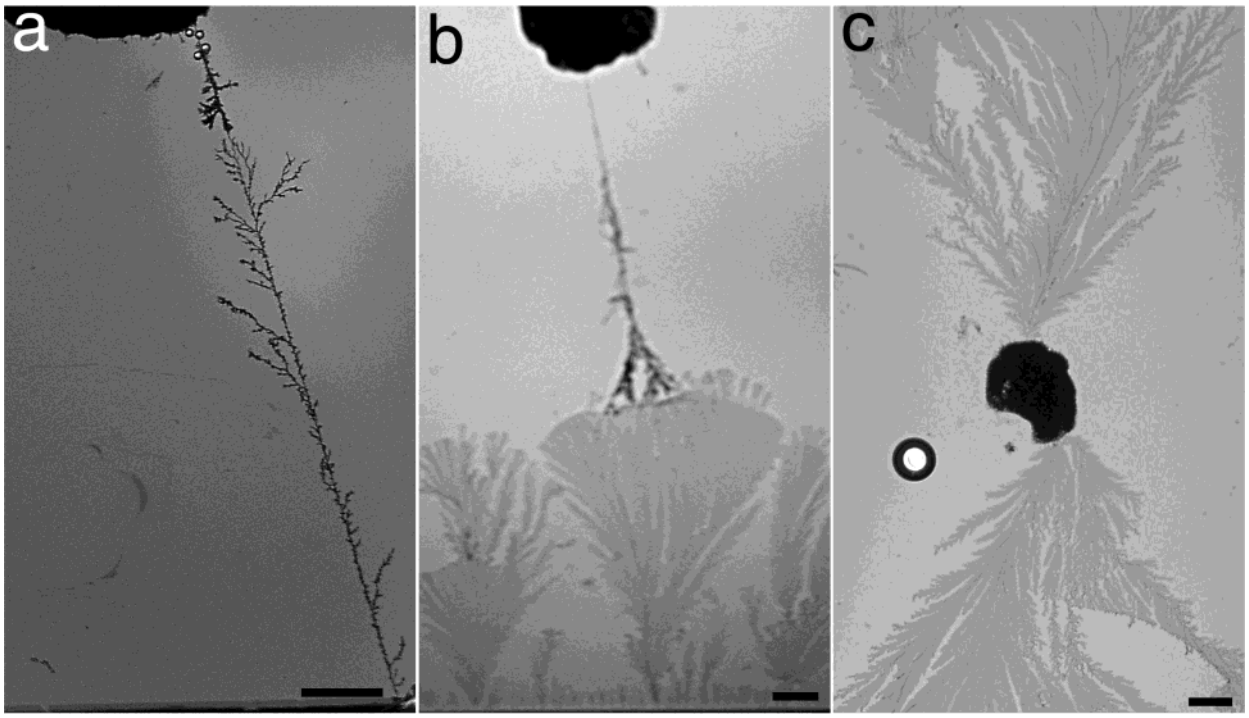

Figure 9. Various types of microwire electrical connections to conductive islands between the electrodes. Islands connected through (a) bulk microwire growth only, (b) a combination of bulk and surface growth, or (c) surface assembly only. Scale bars: 500 μm.

as the growing wires from the opposing electrodes approached each other, to avoid transition to bulk mode and thus achieve complete surface assembly.

The bulk microwires are stable as long as they remain in the liquid phase. However, they do not survive the drying process: the large capillary forces exerted on the long thin fibers by the withdrawing meniscus of the liquid typically lead to breakage and fragmentation. Thus, the bulk wires are limited in application to *in situ* assembly and functions in a liquid environment. This still makes them useful in devices such as biochips and sensors. The surface microwires reported here, however, are mechanically supported by the glass surface. These microwires remain intact even after removal and drying of the liquid phase. This important advantage opens a range of applications of these structures in novel materials. For example, arrays of parallel microwires similar to the ones shown in Figure 8 can be used in materials that conduct electricity and heat in one specific direction or transmit light of specific polarization. Such arrays could also find use for heat management in MEMS devices and in various microchips.

Another important property of the microwire assembly process is the wiring of conductive islands, which may be, for example, electronic or biological objects. As described in the electrostatic calculations, the microwire growth in such systems will start at the island. Figure 9 illustrates connections to conductive islands in the suspension achieved in various ways—bulk only, bulk−surface, and surface only. This method could be used to connect electrically objects in the suspension and to "grow" an electrical circuit out of them. More complex applications, using parallel surface arrays, may include multiple connections on electrical chips and microcircuits.

VI. Conclusions

Assembly of gold nanoparticles from suspensions into microwires under the influence of an alternating electric field has been investigated. Bulk and surface modes of microwire assembly were observed, and the "switching parameters" allowing forming only one type of structure were identified. The assembly speeds are constant throughout the process and are independent of the electric field intensity. The operating parameters that influence the assembly speed and the surface density of the microwires were identified, and the effect of these parameters on the microwire growth process was studied. Electrostatic modeling allowed us to simulate the mechanism of assembly and to predict the general direction of microwire growth.

On the basis of these results, we can now control the process through a range of operating parameters and engineer the microwire structure as needed. Two "extreme" cases of microwire assembly—single unbranched bulk microwire and arrays of massively parallel surface wires—were demonstrated. We can also make *in situ* electrical connections to objects in the gap between the electrodes. These tools can be useful for nanotechnology applications which require formation of electrical wires between miniature devices in liquid or biological environments, or in interfacing of biological cells with electronic circuits. The process can also be useful in the formation of materials with anisotropic thermal or electrical conductivity.

Acknowledgment. We are grateful to Simon Lumsdon, Kevin Hermanson, and Eric Kaler for their contribution to the previous microwire research. This study was supported from grants from the National Science Foundation (NER and CAREER) and the Camille and Henry Dreyfus Foundation.

LA0349976